Spatial accumulation of salicylic acid is in effector-triggered immunity of potato against viruses regulated by RBOHD

Tjaša Lukan[1,*], Maruša Pompe-Novak[1,*], Špela Baebler[1,*], Magda Tušek-Žnidarič[1], Aleš Kladnik[2], Maja Križnik[1], Andrej Blejec[1], Maja Zagorščak[1], Katja Stare[1], Barbara Dušak[1], Anna Coll[1], Stephan Pollmann[3], Karolina Morgiewicz[4], Jacek Hennig[4], Kristina Gruden[1]

*-shared first authorship

[1]National Institute of Biology, Večna pot 111, 1000 Ljubljana, Slovenia
[2]Biotechnical Faculty, University of Ljubljana, Jamnikarjeva 101, 1000 Ljubljana, Slovenia
[3]Centre for Plant Biotechnology and Genomics, U.P.M. - I.N.I.A., Campus de Montegancedo, Crta. M-40, Km 38, 28223 Pozuelo de Alarcón, Madrid, Spain
[4]Institute of Biochemistry and Biophysics, Polish Academy of Sciences, Pawińskiego 5a, 02-106 Warsaw, Poland

Corresponding author: Tjaša Lukan (tjasa.lukan@nib.si).

SIGNIFICANCE

To get towards sustainable resistance in the field, it is important to understand mechanisms of immune signaling. We here show novel aspects of spatial regulation in effector-triggered immunity (ETI) against potato virus Y. A detailed spatiotemporal analysis in and surrounding the foci of viral infection, on ultrastructural, biochemical and gene expression levels revealed that redox state maintenance is tightly spatiotemporally regulated. We also show the interconnection of salicylic acid and RBOHD through a feedback loop, regulated through UDP-glucosyltransferase, revealing the mechanism of this spatial regulation. The proper function of this loop is essential for successful ETI leading to viral arrest.

ABSTRACT

While activation of resistance (R) proteins has been intensively studied, the mechanisms acting downstream of R protein activation remain elusive. We studied effector-triggered immunity (ETI) conditioned by the potato Ny-1 gene against potato virus Y. Transcriptomic, ultrastructural and biochemical analyses of four consecutive tissue sections in and surrounding the foci of viral infection at three different lesion developmental stages revealed processes that are spatiotemporally regulated. The transcriptional response in the cell death zone and surrounding tissue is dependent on SA. For

some of the genes, spatiotemporal regulation is completely lost while for others, the regulation is different in SA-deficient line indicating multiple connections between hormonal signaling modules. The induction of RBOHD NADPH oxidase expression, together with expression of Thioredoxin H gene, occurs specifically in the border region of the lesion during ETI. In plants with silenced RBOHD, ETI is perturbed and virus spread is not arrested at the site of infection. Expression of RBOHD is under the control of SA. On the other hand, RBOHD activity is required for spatial regulation of SA accumulation. We identified an UDP-glucosyltransferase, encoding an enzyme involved in feedback activation of SA biosynthesis, that is derepressed at the border of the lesion in RBOHD silenced plants. Altogether, we revealed a novel aspect of viral ETI, the RBOHD-SA feedback loop required for its spatial regulation.

INTRODUCTION

Plants have evolved sophisticated mechanisms to perceive pathogen attack and effectively respond, either passively or by multi-layered actively-induced immune system. The first layer, pathogen-associated molecular-pattern-triggered immunity (PTI), is based on the recognition of pathogen surface components, common for a number of pathogens, by the plant pattern recognition receptors. The more specific layers of immunity are mediated by intracellular resistance (R) proteins (Jones and Dangl, 2006). R proteins confer recognition of pathogen-derived effectors and initiate effector-triggered immunity (ETI). One of the manifestations of a successful immune response is the hypersensitive response (HR)-conferred resistance, where restriction of pathogens to the infection site is associated with a form of localized programmed cell death (PCD) that leads to the appearance of macroscopically visible localized tissue necrosis (Künstler et al., 2016). HR-conferred resistance is preceded by a series of biochemical and cellular signals. One of the earliest hallmarks of HR is the rapid and intense production of reactive oxygen species (ROS) (Balint-Kurti Peter, 2019). Salicylic acid (SA) is required for the restriction of pathogens during HR in various pathosystems including viruses (Mur et al., 2008; Künstler et al., 2016; Calil and Fontes, 2017) such as tobacco-tobacco mosaic virus (TMV) (Chivasa et al., 1997; Chivasa and Carr, 1998) and potato-potato virus Y (PVY) (Baebler et al., 2014; Lukan et al., 2018). The effectiveness of downstream events in ETI is regulated also by jasmonic acid (JA) and ethylene (ET). Other hormones were also shown to play important roles in plant immunity (Verma et al., 2016). Activation of immune signaling network results in the induced expression of actuators of

defense, such as pathogenesis-related protein 1 (PR1) and beta-glucosidases yet their function is not fully understood (Breen et al., 2017). HR associated PCD was shown to restrict pathogen spread in some biotrophic pathosystems (Dickman and Figueiredo, 2013). It has been however shown that it is not required for resistance in several viral pathosystems (reviewed in Künstler et al., 2016), including potato-PVY interaction (Lukan et al., 2018).

Precise temporal and spatial coordination of induced signaling pathways is required to successfully restrict the pathogen with minimal damage to the host tissue (reviewed in Künstler et al. 2016). The concentric spread, typical of many viruses, results in foci containing cells at different stages of infection (Yang et al., 2007; Rupar et al., 2015). The immune response signal is however transferred to the surrounding tissue, resulting in gradient of response in surrounding cells (Dorey et al., 1997; Havelda and Maule, 2000; Maule et al., 2002; Yang et al., 2007).

PVY, a member of *Potyvirus* genus from family *Potyviridae*, is the most harmful virus of cultivated potatoes (Karasev and Gray, 2013) and among top 10 most economically important viruses infecting plants (Scholthof et al., 2011). The most studied type of resistance to PVY is HR-conferred resistance (Karasev and Gray, 2013). In potato cv. Rywal, HR is initiated by *Ny-1* gene and is manifested as the formation of necrotic lesions on inoculated leaves (Szajko et al., 2008). We have shown previously that the transcriptional dynamics of genes known to participate in the immune response is crucial for the efficient resistance response and that SA is the key component in the orchestration of these events (Baebler et al., 2014).

To dissect the mechanisms acting downstream of Ny-1 R protein activation in ETI we analyzed the processes in lesion development in spatiotemporal manner on the ultrastructural, biochemical and gene expression levels. To evaluate the position of SA in the signaling cascade we in parallel analyzed the responses in SA-depleted NahG plants. We show that SA regulates expression of several immune-related genes in different ways but its lack does not influence the establishment of PCD. We also show that expression of few genes is induced only in the border region of viral foci, the most pronounced is the spatial profile of *RBOHD* gene. Indeed, silencing of *RBOHD* breaks the resistance, allowing systemic

viral spread, which confirms that RBOHD is a regulatory hub in potato ETI. SA is required for efficient regulation of RBOHD, and conversely, RBOHD is required for spatial regulation of SA biosynthesis. RNA-Seq analysis of lesion and the adjacent tissue revealed that UDP-glucosyltransferase UGT76D1, an enzyme participating in feedback activation loop of SA biosynthesis, is under regulation of RBOHD. As SA is modulating the response of genes participating in JA and ET signaling in diverse spatiotemporal manner, we conclude that the efficient ETI is a result of tightly interconnected hormonal network.

RESULTS

ETI-triggered transcriptional response of immune signaling-related genes is diversely spatially regulated at the stage of fully developed lesions

The symptoms development in HR interaction of potato inoculated with $PVY^{N\text{-}Wilga}$ (cv. Rywal, hereafter NT) and its transgenic counterpart depleted in accumulation of SA (NahG-Rywal, hereafter NahG) was as previously described (Baebler et al., 2014; Lukan et al., 2018). In both genotypes symptoms developed as spot necrosis (lesions) on inoculated leaves at 3 days post inoculation (dpi) with $PVY^{N\text{-}Wilga}$ and became fully developed at 5-6 dpi, when lesions reached their final number (Supplemental Figure 1). While ETI was successful in cv. Rywal and the virus was restricted to inoculated leaves, depletion of SA rendered NahG plants susceptible allowing the viral spread throughout the plant accompanied with strong symptom development (Supplemental Figure 1). Here, we additionally analyzed the phenotype of symptoms of both genotypes in interaction with two other PVY strains, PVY^{NTN} and PVY^{N605}, tagged with green fluorescent protein (PVY^{N}-GFP). Symptoms development phenotype and viral multiplication did not differ between the three viral strains on inoculated leaves as well as for upper non-inoculated leaves (Supplemental Figure 1). We also measured the number of palisade mesophyll cells in cross-section through the centre of fully developed lesions, which was 14-20 cells in NT and 20-30 cells in NahG plants. In parallel, we measured lesion diameter in both genotypes and confirmed almost 2-fold larger lesion diameter in NahG-Rywal plants (Supplemental Figure 2).

Previously, we performed a non-targeted transcriptional analysis of inoculated homogenized leaves at 1, 3 and 6 dpi (Baebler et al. 2014). While conducting several additional experiments, we observed that responses can vary between plants, also related to the number of lesions formed on the leaves. Thus,

in-depth biological interpretation of such data is difficult. We thus hypothesized that more detailed spatial analysis of responses would provide better insights into the processes involved in ETI downstream Ny-1 activation. We developed the protocol for reliable sampling of tissue sections surrounding the lesion at different stages of lesion development (Figure 1A) and adapted RNA extraction to allow work with minute amounts of tissue. As the amounts of RNA obtained from individual small tissue sections are limited, we selected 23 genes for our analysis according to their biological function and responsiveness in our microarray dataset (Baebler et al. 2014; Supplemental Table 1). These selected genes were chosen due to their specific role in immune signaling: in redox potential homeostasis (*CAT1*, *PRX28*, *RBOHD*, *RBOHA*, *RBOHC*, *TRXO*, *TRXH*), cell death (*MC3*, *LSD1*), RNA silencing (*AGO2*, *SAHH*), MAP kinase cascade (*WIPK*, *MKP1*), SA (*TGA2*), JA (*13-LOX*, *9-LOX*, *ACX3*), ET (*ERF1*) or auxin (*ARF2*) signaling, actuators of defense (*BGLU*, *PR1B*) or as markers for primary metabolism state (*GBSSI*) (Figure 1B). In parallel to gene expression of those genes, the relative amount of PVY RNA was measured as well (Supplemental Datasets 1 and 2).

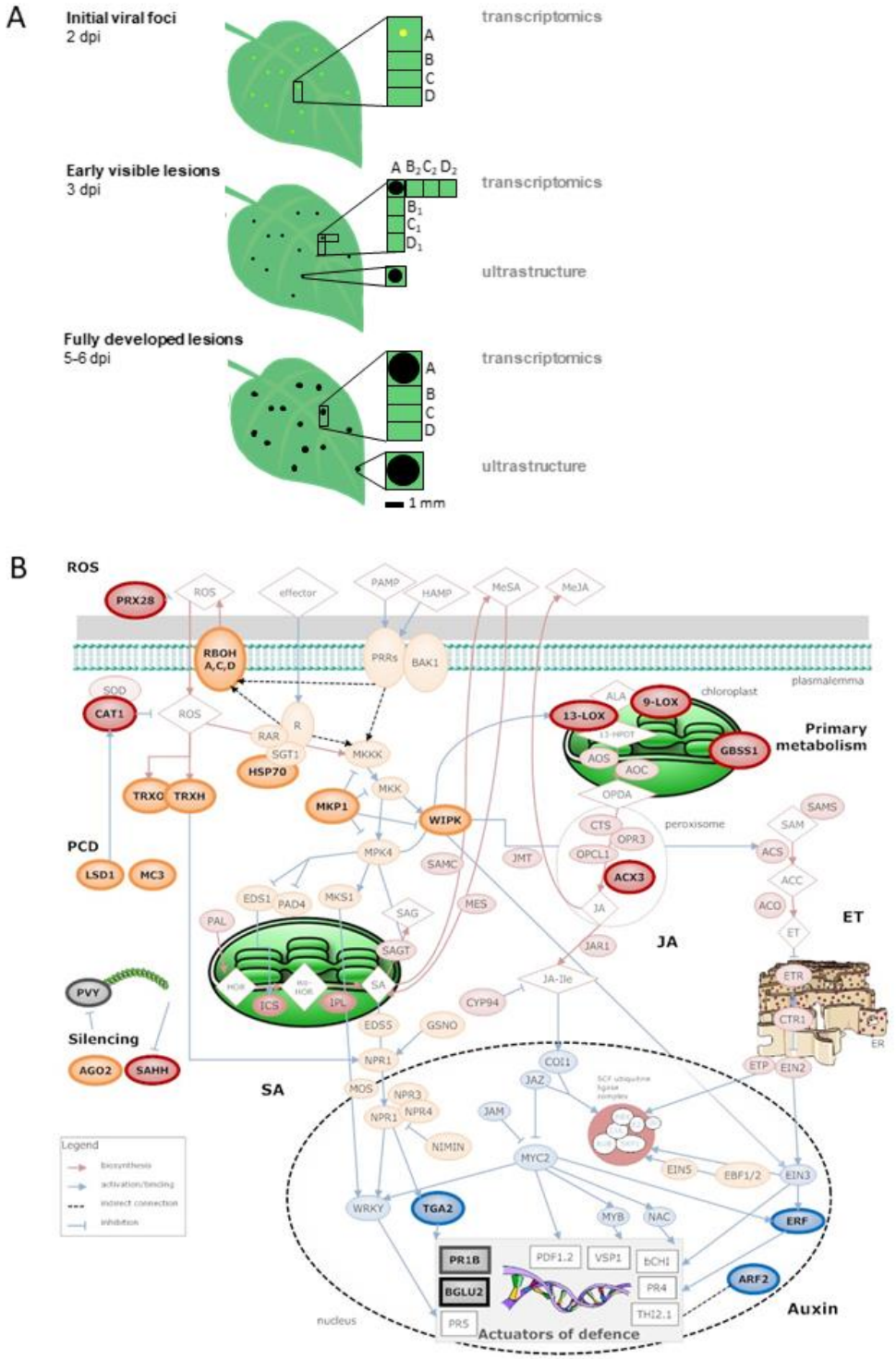

Figure 1: Plant immune signaling-related genes selected for transcriptomic spatiotemporal response analysis. A) Experimental setup. Sections containing initial virus foci (section A) and surrounding tissues (sections B, C and D) were sampled for transcriptomics and electron microscopy at different time points. Tissue surrounding early visible lesions was sampled in two perpendicular directions, here marked with 1 and 2, respectively. Scale bar: 1mm. B) Selected plant immune signaling-related genes. Potato virus Y (PVY)

accumulation and expression of genes involved in reactive oxygen species (ROS), MAP kinase signaling, programmed cell death (PCD), salicylic acid (SA), jasmonic acid (JA), ethylene (ET), auxin and primary metabolism were analyzed (bold border). Signaling proteins are presented as orange, enzymes as red and transcription factors as blue ovals, respectively; metabolites are presented as diamonds and genes as squares. 13-LOX: 13-lipoxygenase, 9-LOX: 9-lipoxygenase, ACX3: acyl-CoA oxidase, AGO2: argonaute 2, ARF2: auxin response factor 2, BGLU2: 1,3-beta-glucosidase, CAT1: catalase 1, ERF1: potato ethylene responsive transcription factor 1a, GBSS1: granule-bound starch synthase 1, HSP70: heat shock protein 70, LSD1: zinc finger protein LSD1, MC3: metacaspase 3, MKP1: mitogen-activated protein kinase phosphatase 1, PR1B: pathogenesis-related protein 1b, PRX28: peroxidase 28, RBOHA: potato respiratory burst oxidase homologue A, RBOHC: potato respiratory burst oxidase homologue C, RBOHD: potato respiratory burst oxidase homologue D, SAHH: adenosylhomocysteinase S-adenosyl-L-homocysteine hydrolase, TGA2: bZIP transcription factor family protein, TRXH: thioredoxin H, TRXO: thioredoxin O, WIPK: potato wound inducible protein kinase. See Supplemental Table 4 for gene IDs and primer information.

First, we analyzed fully developed lesions following the infection with $PVY^{N\text{-}Wilga}$ (Figure 1A). Indeed, reproducibility of these results was between lesions of different plants and even of independent biological experiments much higher than when performing analysis of whole leaf homogenates (Figure 2). We also performed experiments with two additional viral strains, PVY^{NTN} and PVY^{N} and observed the same response profiles (Supplemental Figure 3). While there was most of viral RNA in the centre of the lesion in both potato genotypes, the expression pattern of genes changed with distance from the centre of the lesion and in some cases, the response was different between the two genotypes (Figure 2). To simplify the visualization and interpretation of spatial response comparisons among different genes within the two genotypes, we designed coefficient plots, condensing the information of spatial response to pairs of quadratic and linear coefficient values from the polynomial model fit (Figure 2, bottom position). The expression of *HSP70* (see Figure 1B for full gene names) encoding a protein involved in the stability of R proteins (Kadota and Shirasu, 2012), is elevated in the centre of viral foci (section A) compared to the adjacent sections (sections B, C and D) only in non-transgenic (NT) plants (Figure 2). Both, *BGLU2* and *PR1B* (Figure 2) are also under the regulation of SA signaling pathway. While they indeed show strong upregulation close to the centre of viral infection (more than 10-fold compared to the distal tissue, D section) during ETI, their response quite differs in SA-depleted system. While the spatial response of *BGLU2* in NahG plants is completely lost, the peak of *PR1B* response is occurring further away from the foci of viral infection (peak in section C, Figure 2). The regulation of *ERF1*, involved in ET signaling, resembles the one of *PR1B* in both genotypes. The starch synthase *GBSS1*, an indicator of primary metabolism state, shows that the metabolism is downregulated in the

centre of the lesion, while in section D, its expression status is closer to the one in mock-inoculated leaf tissue (Figure 2, denoted with empty circles at the right end of x-axis). This is however not true in NahG plants where the expression of *GBSS1* is downregulated further away from the lesion (Figure 2).

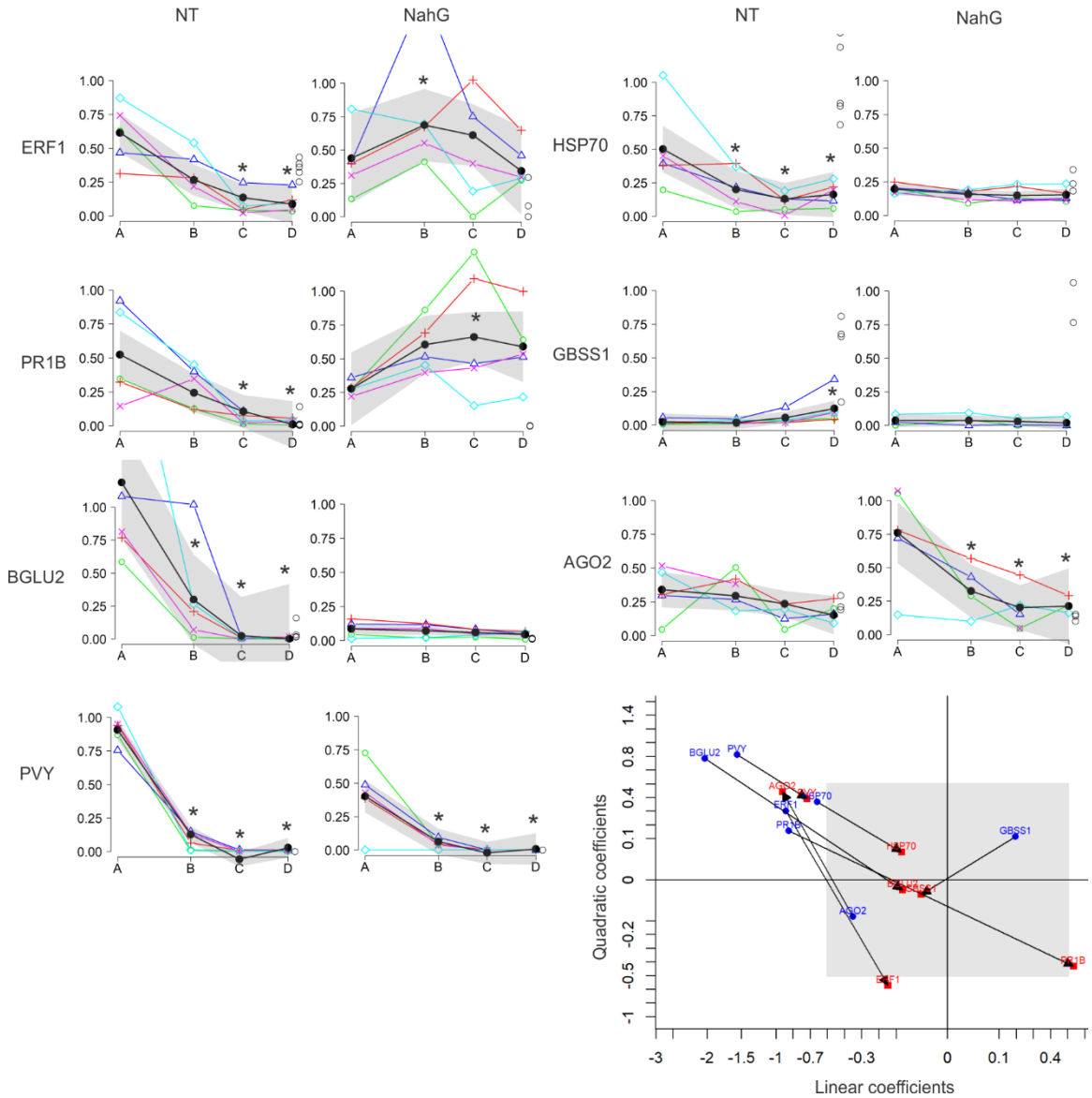

Figure 2: The lack of SA leads to diverse spatial transcriptional regulation of immune-related genes in ETI. Transcriptional profiles of the selected genes were monitored in non-transgenic (NT) and SA-depleted (NahG) plants following inoculation with PVY$^{N\text{-}Wilga}$ at the stage of fully developed lesions (top position). Tissue sections, marked as positions A, B, C, D, are shown on the x-axis and values of gene transcriptional response standardized to 97th quantile on the y-axis. Expression values in mock-inoculated tissue sections are shown as empty circles on the right end of x-axis. Asterisk denotes statistical significance (p-value < 0.05) of gene expression at position B, C and D compared to that at position A. Spatial profile models are shown as thick black lines with 95% confidence interval bands in grey. Standardized gene expression values within individual lesions

are presented with colored symbols connected by a line. To simplify the visualization and interpretation of spatial response comparisons among different genes within different genotypes, we designed coefficient plots (plotted pairs of quadratic and linear coefficient values from the polynomial model fit, bottom right position). Value pairs for NT are shown as blue circles, value pairs for NahG as red squares. Grey box defined within [-0.5,0.5] interval boundaries indicates an area of lower relevance regarding the difference in gene expression response. Full gene names are given in the legend of Figure 1B.

We also show that expression of genes involved in JA biosynthesis, maintenance of redox potential and the ones involved in cell death is spatiotemporally regulated, which is presented in more detail in next subchapters. The rest of the analyzed genes showed either no spatial regulation at all or they were responding in an asynchronous manner between the biological replicates (Supplemental Datasets 1 and 3), meaning that most probably their regulation is even more fine-tuned and more detailed analysis (e.g. with single cell resolution) would be required.

Next, we wanted to implement our approach in the earlier stages of viral infection. Using PVY^N tagged with GFP, we tried to visualize cells that are only starting to amplify the virus but the virus has not spread for more than 5 cells (Figure 1A). Such an approach has proved very demanding due to high background fluorescence in potato and the fact that PVY is not multiplied in an individual cell to a high extent. We performed two independent experiments and were able to isolate initial foci of infection in only one of them. We tested each of the sampled foci of infection for true PVY multiplication and had to discard 2 out of 5 foci for both genotypes, as the fluorescence observed was most probably due to inoculation-triggered accumulation of phenol compounds in potato leaf trichomes (Supplemental Figure 4). The spatial expression profiles for the remaining lesions were less reproducible (Supplemental Figure 5, Supplemental Dataset 2). The reason might be that due to the smaller number of infected cells at the stage of initial viral foci, sampling did not allow for distinction between the physiological conditions (sections A and B in fully developed lesions). Biological interpretation of this data is thus not possible.

As the first robust time point for spatial analysis of responses, we identified the early visible lesions, these are lesions visible only when leaves are transilluminated and are of 0.5-1 mm in diameter (Figure 1A). Indeed, when comparing the response profiles of different lesions and profiles within the same

lesion in perpendicular directions, the results were consistent and enabled reliable biological interpretation (Supplemental Figure 6, Supplemental Datasets 2 and 4). Biological interpretation of the results is presented in next subchapters.

The ultrastructural features of programmed cell death in lesions are not dependent on SA

Our spatiotemporal analysis of gene expression also included two genes involved in regulation of PCD. *MC3* is not transcriptionally regulated (Supplemental Figure 7). *LSD1* showed induction in response already in the early stage of lesion development in both genotypes, albeit stronger in NT plants (Supplemental Figure 7). Its expression was the strongest at the foci of viral infection. To get a better insight into the role of SA in characteristics of PCD, we studied the lesion phenotype also on the ultrastructural level in inoculated leaves of both genotypes after inoculation with $PVY^{N\text{-}Wilga}$ and PVY^{NTN}. In the centre of lesions, the cells were in the final stages of the cell death process, and only the cell wall and a small amount of electron dense material was visible (Supplemental Figure 8). The transition between cells in the last stage of PCD and normal cells was both at the stage of early and fully developed lesions limited to narrow layer of cells. The ultrastructural changes that are characteristic for HR-conferred PCD occurred in all kinds of parenchymal cells, bundle sheath cells as well as in companion cells adjacent to dead cells. In parenchymal and bundle sheat cells vacuolization of cytoplasm, an autophagy feature, was in progress (Figure 3A, C, F), while the cytoplasm of companion cells became electron dense (Figure 3B). Many chloroplasts in companion cells reflected distortion of grana with larger interthylakoidal spaces (Figure 3B), degradation of chloroplasts was also present in mesophyll (Figure 3E) and bundle sheath (Figure 3F) cells. No differences were however observed in characteristics of PCD between both studied genotypes (Figure 3), indicating that the process does not depend on SA.

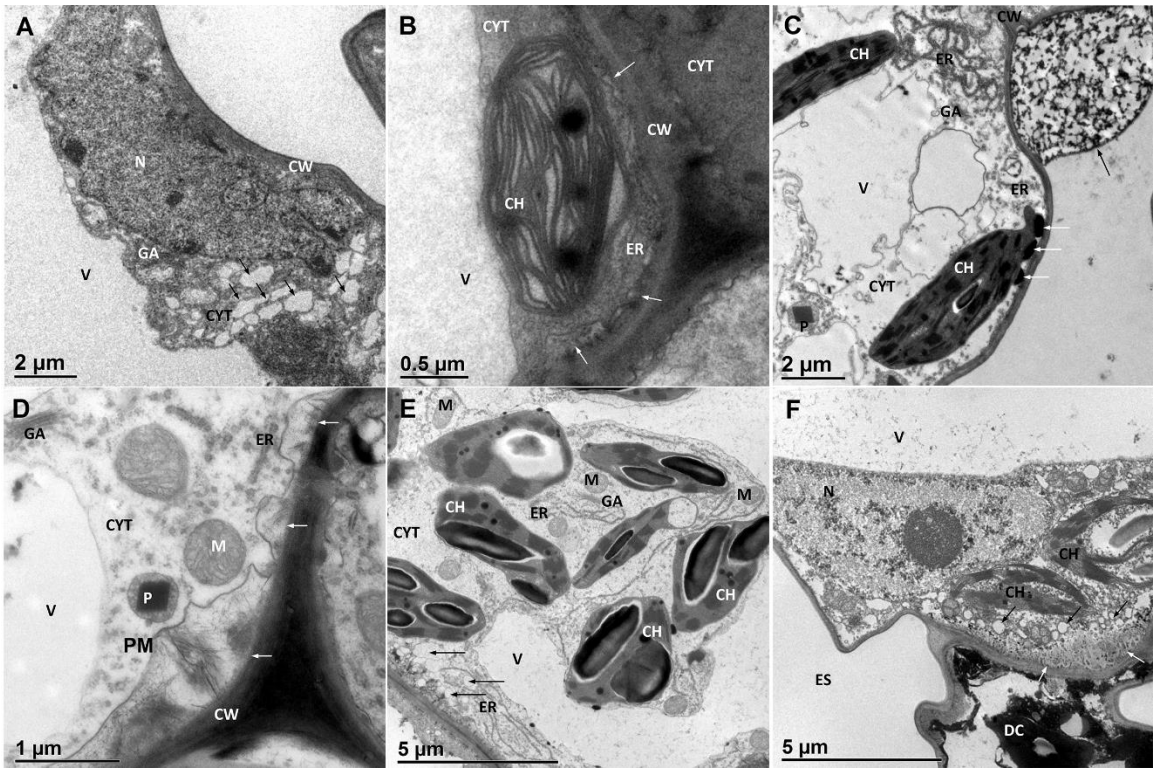

Figure 3: Features of HR-type of programmed cell death are not dependent on salicylic acid. The same features were observed at the border of cell death zone in both non-transgenic (A, B, C) and NahG plants (D, E, F). (A) Ameboidal nucleus and vacuolized cytoplasm in bundle sheath cell. (B) Disorganized thylakoid in chloroplast and detachment of plasmalemma from the cell wall (white arrows) of the companion cell. (C) Highly vacuolized cytoplasm and accumulation of electron dense material inside (white arrows) and outside (black arrow) the cell. (D) Detachment of plasmalemma from cell wall (white arrows) in bundle sheat cell. (E) Degradation of chloroplasts and increased ER in mesophyll cell. (F) Detachment of plasmalemma (white arrows), vacuolization of cytoplasm (black arrows), beginning of chromatin condensation and degradation of chloroplasts in bundle sheat cell. CH: chloroplast, CW: cell wall, CYT: cytoplasm, DC: destroyed cell, ER: endoplasmic reticulum, ES: extracellular space, GA: Golgi apparatus, M: mitochondrion, N: nucleus, P: peroxisome, PM: plasmalemma, V: vacuole.

Expression of JA biosynthesis-related genes is spatiotemporally regulated in potato ETI against PVY

SA is thought to be the main signaling module reprogramming plant in interaction with biotrophic pathogens while JA signaling contributes to a successful defense against necrotrophic pathogens and herbivores. Here we show that *13-LOX* gene, encoding the 13-lipoxygenase starting the oxylipin branch leading to JA biosynthesis, is induced in the centre of viral foci at the stage of fully developed lesions (Supplemental Figure 9). The response is, in agreement with the hypothesis that JA and SA are antagonistic, enhanced in NahG plants. The expression pattern of *ACX3* gene, involved in later steps of JA biosynthesis (Figure 1B), is regulated similarly, except for the diminished regulation at the stage of fully developed lesions of NahG plants (Supplemental Figure 9). Interestingly however is that gene expression of *9-LOX*, coding for the starting enzyme of the second branch of oxylipin pathways, is not following the same spatiotemporal response as *13-LOX* gene expression (Supplemental Figure 9).

Expression of genes involved in redox state maintenance is tightly regulated across the studied spatiotemporal scale

We also extensively investigated the genes involved in generation and quenching of ROS (Figure 1B). We studied three *RBOH* genes, involved in generation of apoplastic ROS and leading to redox changes in the cytoplasm. On the quenching side, we analyzed gene expression of CAT1, located in the peroxisome, and apoplastic peroxidase PRX28. Additionally, we monitored the gene expression of two cytoplasmic redox potential sensor proteins that were implicated in the regulation of immune signaling, thioredoxins H and O (TRXH and TRXO). The three investigated *RBOH* genes have each distinct spatiotemporal regulation. *RBOHC* is not regulated in any of the studied genotypes (Figure 4). *RBOHA* is strongly induced in the centre of viral foci already in early stage of lesion development and goes back to normal in section B in NT, while this activation is attenuated in NahG plants. *RBOHD*, however, responds in section A in early stages while later on, it forms a peak of expression close to the border of the lesion itself in the majority of lesions. *RBOHD* is also under regulation of SA as this gene is expressed close to the limit of quantification in NahG plants. *PRX28* is induced earlier in NahG plants, and at the stage of fully developed lesion its expression peaks in section A in NT and in section B in NahG plants. *CAT1* is induced only in NahG plants and is induced even further away from the centre of viral foci compared to *PRX28*. At the stage of early lesions, it peaks in section C and at the stage of fully

developed lesions even in section D. The expression of *TRXO* was below the limit of quantification, therefore, it was not possible to follow its response. Interestingly, however, *TRXH* responds strongly and early only in NT plants.

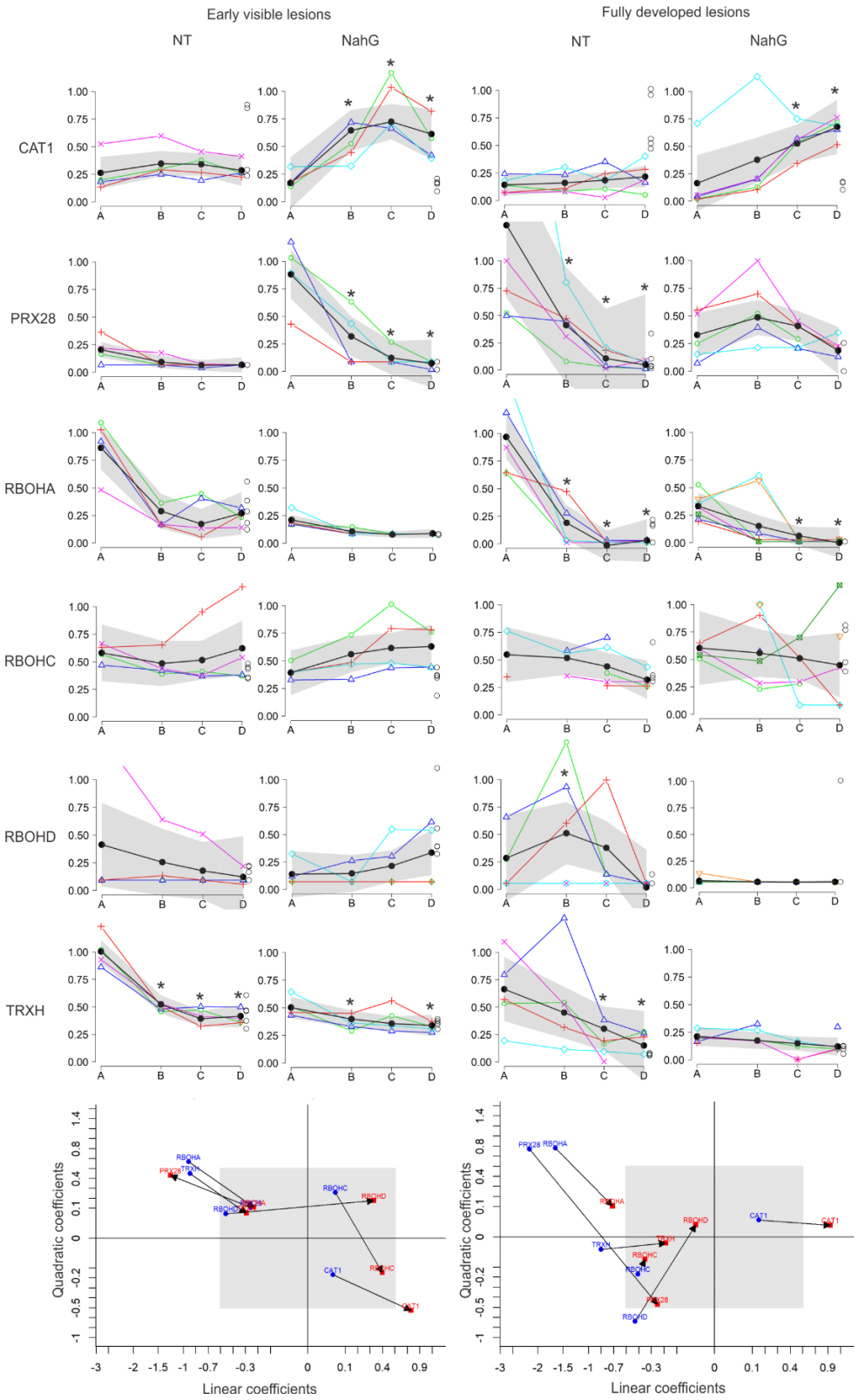

Figure 4: Induction of expression of *RBOHD* and *TRXH* is limited to the cells surrounding the infected tissue. Spatial expression profiles of selected genes (top position) and coefficient plots (bottom position) for non-transgenic (NT) and SA-depleted (NahG) plants after inoculation with PVY$^{N\text{-}Wilga}$ at the stage of early visible (3

dpi, left, averaged profile of the two perpendicular directions) and fully developed lesions (5-6 dpi). See Figure 2 legend for the full description of the graphs and Figure 1B for full gene names.

ROS generation is limited in ETI but not if SA is depleted from the system

We further wanted to inspect how changes in transcriptional activity of ROS-related genes are reflected in accumulation of H_2O_2. We followed H_2O_2 production in relation to lesion size in several time points following virus inoculation. In contrast to visible lesion growth pattern (Figure 5A), the H_2O_2 accumulation area around the lesions was significantly larger in NahG plants after 5 dpi (Figure 5B). Interestingly, the stained area was continuously increasing in NahG plants, while it reached a plateau in NT plants, indicating that ROS production is limited around the lesions in plants exhibiting functional ETI, but not in SA-depleted plants (Figure 5C).

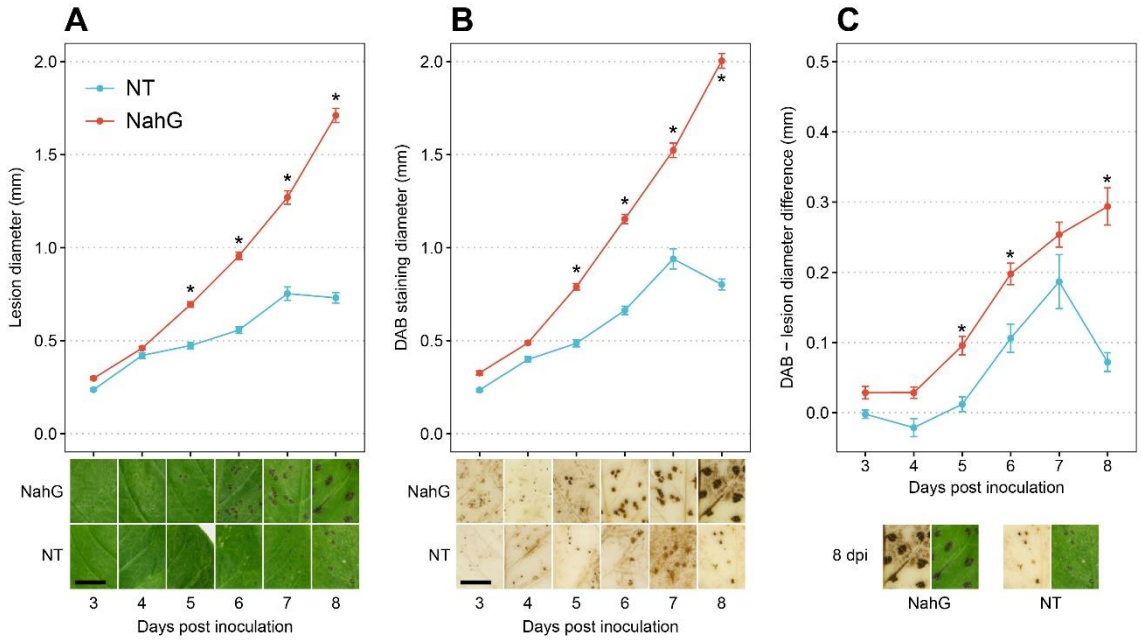

Figure 5: H_2O_2 accumulation is continuously stronger during infection with PVY in potato plants perturbed in SA signaling. (A) Lesion diameter was significantly larger in the NahG plants from 5 dpi on compared to non-transgenic (NT) ones. (B) DAB staining indicating H_2O_2 activity (visible as the brown precipitate) was significantly wider in NahG plants from 5 dpi on, if compared to NT plants. (C) Difference in diameter of DAB staining and the diameter of the corresponding lesion showing that in NahG plants the H_2O_2 positive area outside the lesion is wider in comparison to NT plants. The representative areas of leaf images and comparison of lesion and DAB staining at 8 dpi are shown under the plots (bar represents 10 mm). Asterisks represent statistically significant differences between the two genotypes at the same day ($p < 0.05$). Error bars represent standard error.

Functional *RBOHD* is indispensable for the *Ny-1* gene-mediated ETI

RBOHD showed a specific spatiotemporal expression profile, peaking at the border of virus amplification zone (Figure 4). To validate the involvement of ROS signaling and specifically *RBOHD* gene in virus restriction, we constructed transgenic plants of cv. Rywal with silenced *RBOHD* gene (shRBOHD; Supplemental Figure 10). We inoculated two independent transgenic lines of shRBOHD (lines 13 and 14) with PVY^N-GFP as the least virulent PVY strain among the ones used in this study (Lacomme et al., 2017). The virus spread systemically and lesions appeared in upper, non-inoculated leaves (Figure 6A, Supplemental Figure 10). Time of first lesion appearance in upper, non-inoculated leaves was comparable to the time of first lesion appearance in NahG plants, but the viral RNA amounts were lower than in NahG plants (Supplemental Figure 10).

We also checked if the virus can multiply to a larger extent in the inoculated leaves of shRBOHD plants. We detected viral RNA in inoculated leaves of shRBOHD plants, however in lower amounts than in NahG plants (Figure 6C). The viral amount negatively correlated ($r = -0.85$) with *RBOHD* expression taking into account all analyzed genotypes (Figure 6B; Supplemental Figure 11).

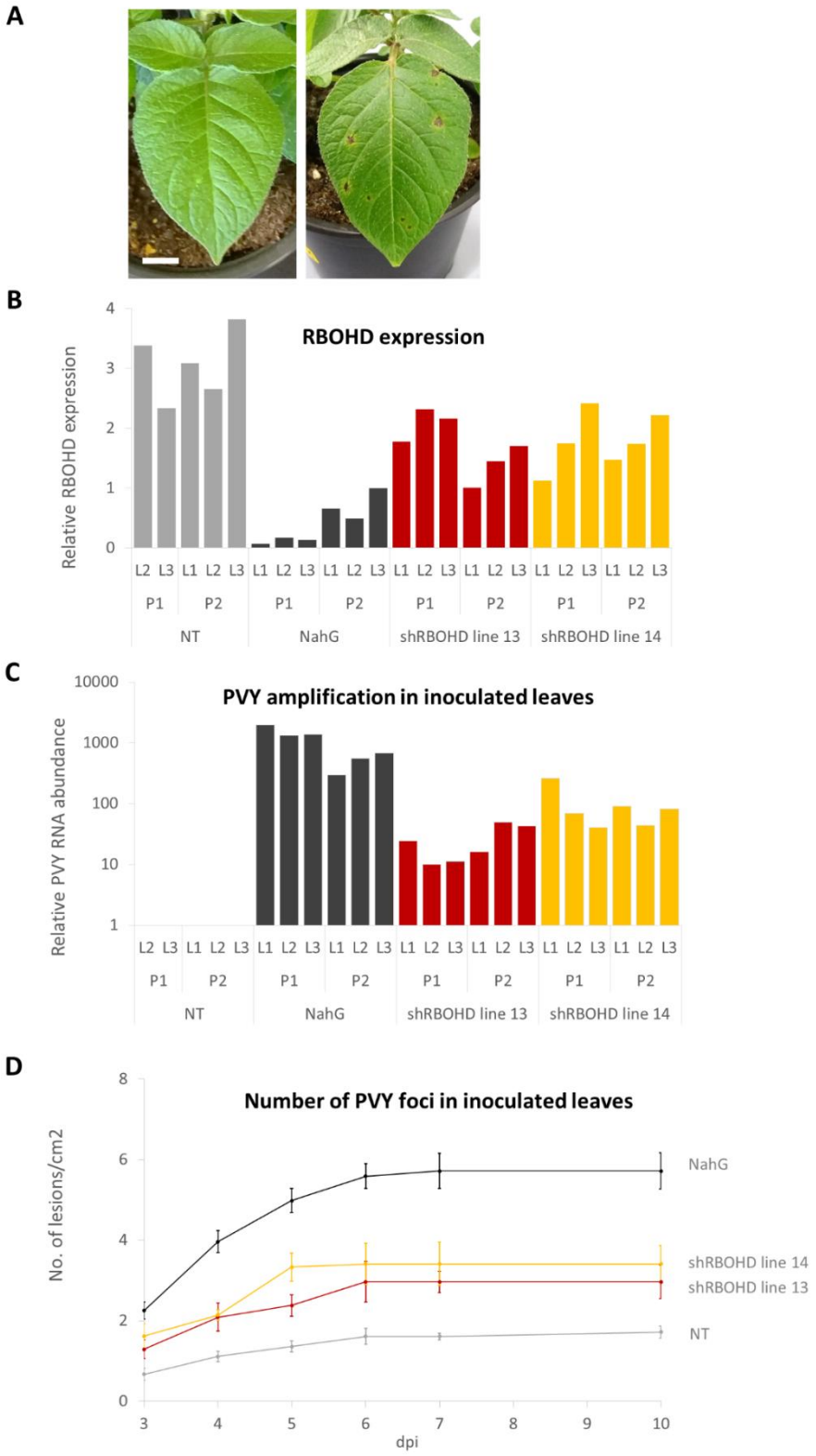

Figure 6: **Virus efficiently multiplies in plants with silenced *RBOHD* gene**. (A) Lesions on non-inoculated leaf of *RBOHD*-silenced plant of transgenic line 14 (right) and non-transgenic counterpart (left) 17 dpi. Scale bar is 1 cm. (B) Relative *RBOHD* expression in inoculated leaves 6 dpi. (C) Relative PVY RNA abundance (relative to

the lowest detected viral amount, shown on a logarithmic scale) 6 dpi in NT, NahG and shRBOHD plants. P: plant number, L: leaf number (D) Number of lesions per cm^2 as they appeared on the youngest inoculated leaves of plants (n = 6 – 10) of different genotypes at particular dpi. Error bars represent the standard error of the number of lesions per cm^2. Individual measurements are available in the Supplemental Dataset 5.

We additionally followed a number of lesions appearing on the inoculated leaves in the two *RBOHD*-silenced transgenic lines after inoculation with PVY^N-GFP in comparison with NT and NahG plants. We observed an increased number of viral foci on inoculated leaves of shRBOHD plants in comparison to NT plants (Figure 6D, Supplemental Figure 11). On the other hand, the number of lesions in shRBOHD plants was lower if compared to NahG plants (Figure 6D, Supplemental Figure 11). We conclude that the RBOHD contributes to blocking of viral multiplication within the cell and thus establishment of foci of viral infection.

RBOHD is involved in tight spatial regulation of SA accumulation during ETI

ROS were shown to be involved both upstream and downstream of SA signaling (Herrera-Vasquez et al., 2015). To determine if RBOHD-generated ROS are involved in regulation of SA signaling in ETI, we analyzed SA induction in shRBOHD plants. In the pool of lesions (section A), SA was induced to the same extent as in RBOHD-silenced plants (approximately 10-fold compared to mock samples; Figure 7, Supplemental Table 2), while in the surrounding cells (pool of sections B) accumulation was lower in non-transgenic plants but not in RBOHD-silenced plants. Since the concentration of SA in transgenic plants did not differ significantly from the concentration in non-transgenic plants in the lesion (Figure 7), we conclude that RBOHD-generated ROS are not involved in the induction of SA biosynthesis. However, the tight spatial regulation of SA biosynthesis was lost in shRBOHD plants. Additionally, we know that *RBOHD* gene activity is under regulation of SA as the expression of this gene is much lower in NahG plants after virus inoculation (Figure 6B, Supplemental Figure 10, Supplemental Dataset 1). Interestingly, the JA content was under the limit of quantification in all of the pooled small tissue sections samples, indicating that strong induction of JA biosynthesis is occurring neither in the lesion nor in the vicinity of the lesion.

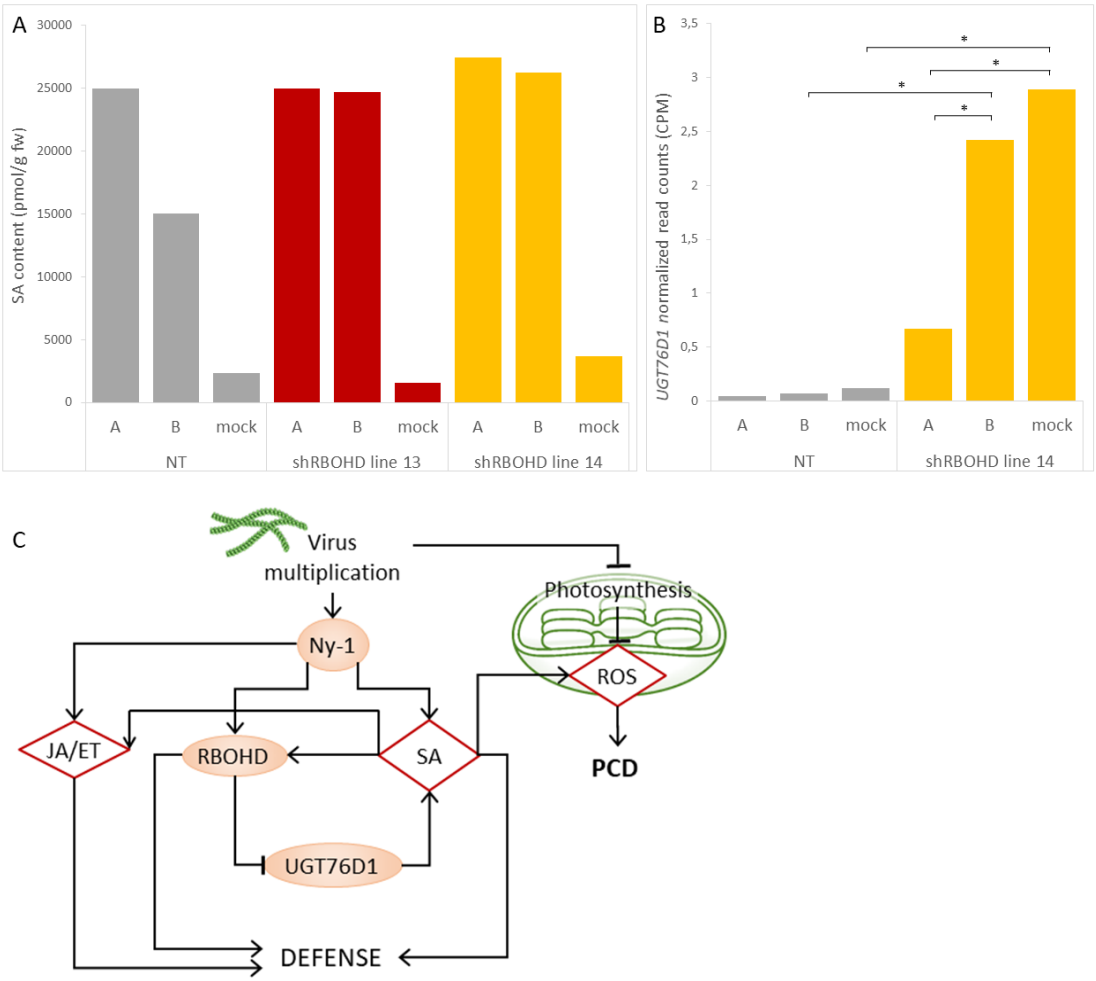

Figure 7: Functional *RBOHD* contributes to spatial regulation of SA accumulation in potato ETI against PVY. A) SA content was measured in the early stage of lesion development in non-transgenic (NT) and RBOHD-silenced plants (shRBOHD) within the lesion (section A) and in the tissue surrounding the lesion (section B) in comparison to mock-inoculated sections. Pools of 50-100 tissue sections from 6-8 plants were analyzed. Detailed data is shown in Supplemental Table 2. B) Expression of *UDP-glucosyltransferase* (*UGT76D1*) within the lesion (section A), its close surroundings (section B) and sections of mock-inoculated plants of NT and shRBOHD plants, as determined by RNA-Seq analysis. The bar graph is showing the average normalized read counts (CPM) of UGT76D1 gene across three biological replicates. Asterisks represent statistically significant differences among comparisons (FDR adj. p-value < 0.05). C) SA synthesis and RBOHD are interconnected through regulatory loops. Salicylic acid (SA) regulates potato respiratory burst oxidase homologue D (RBOHD) expression and on the other hand, RBOHD is, through UDP-glucosyltransferase (UGT76D1), involved in spatial distribution of SA accumulation. Signaling proteins are presented as orange ovals and metabolites as red diamonds. JA/ET (jasmonic acid/ethylene signaling), ROS: redox oxidative species, PCD: programmed cell death, Ny-1: R protein.

We have further explored the mechanisms underlying spatial regulation of SA accumulation on the border of the lesion. We performed a RNA-Seq analysis of the tissue within the lesion (section A) and the adjacent tissue (section B) at the time of early visible lesions for all three genotypes, NT, NahG and shRBOHD. This analysis provided insights into processes regulated by SA or RBOHD (Table 1, Supplemental Figure 12, Supplemental Dataset 6). The majority of processes spatially differentially regulated overlap between NahG and shRBOHD plants, as *RBOHD* expression is repressed in NahG plants. We however show also that some of the genes and even processes/protein groups are specifically regulated only when *RBOHD* gene is silenced. Most notable regulation is regulation of MYB transcription factors (3 regulated only in the absence of *RBOHD* and not in NT or NahG transgenic plants, Supplemental Dataset 6) and regulation of protein degradation (specific regulation of several proteases as well as ubiquitin SCF and RING E3 ligases, Supplemental Dataset 6). This shows that RBOHD has some additional roles that are independent of SA.

Table 1: *RBOHD* contributes to spatial regulation of processes in potato ETI against viruses. Differentially regulated processes in lesion (A) and tissue surrounding it (B) were compared in non-transgenic plants (NT) and in plants with perturbed SA accumulation (NahG) or reduced *RBOHD* expression (shRBOHD). Only statistically significant (false discovery rate corrected Q-value < 0.05) enriched gene sets determined by gene set enrichment analysis (GSEA) in at least one comparison are presented. ”+“- induced processes, ”–“- repressed processes, blanks denote that a current process was not statistically significantly enriched.

Process (MapMan BIN)	B vs A		
	NT	shRboHD	NahG
1.1.1.1 PS.LIGHTREACTION.PHOTOSYSTEM II.LHC-II	+		+
1.1.1.2 PS.LIGHTREACTION.PHOTOSYSTEM II.PSII POLYPEPTIDE SUBUNITS	+	+	+
1.1.2.2 PS.LIGHTREACTION.PHOTOSYSTEM I.PSI POLYPEPTIDE SUBUNITS		+	+
1.1.6 PS.LIGHTREACTION.NADH DH	+	+	+
1.1.40 PS.LIGHTREACTION.CYCLIC ELECTRON FLOW-CHLORORESPIRATION			+
11.9.4.13 LIPID METABOLISM.LIPID DEGRADATION.BETA-OXIDATION.ACYL COA REDUCTASE	–	–	
13.2.7 AMINO ACID METABOLISM.DEGRADATION.HISTIDINE		–	
16.1.2 SECONDARY METABOLISM.ISOPRENOIDS.MEVALONATE PATHWAY			+
16.8.2.1 SECONDARY METABOLISM.FLAVONOIDS.CHALCONES.NARINGENIN-CHALCONE SYNTHASE			+
20.1.7.3 STRESS.BIOTIC.PR-PROTEINS.PR3/4/8/11 (CHITINASES AND CHITIN BINDING PROTEINS)		–	
26.9 MISC.GLUTATHIONE S TRANSFERASES			–
26.19 MISC.PLASTOCYANIN-LIKE	–	–	–
26.25 MISC.SULFOTRANSFERASE			+
27.3.6 RNA.REGULATION OF TRANSCRIPTION.BASIC HELIX-LOOP-HELIX FAMILY (BHLH)			+
27.3.26 RNA.REGULATION OF TRANSCRIPTION.MYB-RELATED TRANSCRIPTION FACTOR FAMILY		+	
29.2.1.99.99 PROTEIN.SYNTHESIS.RIBOSOMAL PROTEIN.UNKNOWN.UNKNOWN	+	+	+
29.4.1.57 PROTEIN.POSTRANSLATIONAL MODIFICATION.KINASE.RECEPTOR LIKE CYTOPLASMATIC KINASE VII		–	
29.5 PROTEIN.DEGRADATION		+	
29.5.11.20 PROTEIN.DEGRADATION.UBIQUITIN.PROTEASOM			–
29.5.5 PROTEIN.DEGRADATION.SERINE PROTEASE			+
29.8 PROTEIN.ASSEMBLY AND COFACTOR LIGATION	+	+	+
30.11 SIGNALLING.LIGHT		+	+
30.2.17 SIGNALLING.RECEPTOR KINASES.DUF 26			–
31.4 CELL.VESICLE TRANSPORT		–	–
34.1 TRANSPORT.P- AND V-ATPASES			–
34.10 TRANSPORT.NUCLEOTIDES			+
34.13 TRANSPORT.PEPTIDES AND OLIGOPEPTIDES		+	+

We further inspected the RNA-Seq results for any evidence of the feedback loop indicating the role of *RBOHD* in spatial regulation of SA accumulation. We have identified an *UDP-glucosyltransferase* (*UGT76D1,* Sotub10g024000) that is strongly spatially deregulated in RBOHD silenced plants and could be the one directly involved in the process (Figure 7B, Supplemental Figure 13). In line with the evidence that *RBOHD* is repressed in NahG plants, similar expression pattern is observed also in these plants. UGT76D1 is in Arabidopsis implied in feedback activation loop of SA biosynthesis (Huang et al., 2018). Overexpression of this gene led to accumulation of SA. Here we similarly show that silencing of *RBOHD* results in induction of *UGT76D1* gene in section B which explains higher levels of SA detected in B section of transgenic lines (Figure 7).

DISCUSSION

The HR type of resistance is a frequent outcome of ETI. The mechanism of activation of R proteins and their interaction with effectors was the subject of intensive research in recent years (Baggs et al., 2017; Macho and Lozano-Duran, 2019). However, to get towards sustainable resistance in the field where plant is exposed also to other environmental stressors, understanding of downstream processes leading to pathogen arrest is of utmost importance to balance the trade-offs between growth and immunity. To date, most of the studies of those processes were performed for the model plant Arabidopsis (Piquerez et al., 2014). Although some findings can be transferred to crop species using orthology (Lee et al., 2015; Ramšak et al., 2018) this is not always the case as, for example, in recently reported redundancy of *PAD4* in *Solanaceae* (Gantner et al., 2019). Therefore it is important to perform the studies also in crop plants, such as potato.

Pathogen-infected leaf tissue comprises a heterogeneous mixture of host cells in different stages of defense response due to pathogen and defense signal movement from the primary infected cell (Maule et al., 2002). Recently, spatially-resolved transcriptome profiling in plant tissues has gained importance in unravelling complex regulatory networks (Giacomello et al., 2017; Shulse et al., 2019). When homogenized material is used to study the gene expression after virus infection, spatial and to some degree, quantitative information is lost. The progressive and asynchronous effects of viral infection on host gene expression in relation to the spatial distribution of the virus have been investigated previously, but in compatible interactions (Aranda et al., 1996; Escaler et al., 2000; Maule et al., 2002; Yang et al., 2007). In ETI, however, the spatial distribution of a limited number of components has been studied only in model plants. Spatiotemporal response of a single gene in relation to virus spread (Antoniw and White, 1986) and expression of a few genes in only two zones (necrotic and asymptomatic) (Mur et al., 1997) were analyzed in tobacco – TMV interaction. Recently, spatiotemporal dynamics of *PR1* and *Vegetative Storage Protein 1* marker genes' promoter activities were monitored in HR to *Pseudomonas syringae* effector (Betsuyaku et al., 2018). We here followed the expression of 23 genes in four consecutive tissue sections in and surrounding the foci of viral infection, in different developmental stages of HR lesions. To unravel the effects of SA in downstream processes, we in parallel performed all analyses in SA depleted transgenic counterpart. Our approach

for analysis of small tissue sections presents a step forward in studying the ETI against the virus and enabled identification of a novel key player and the interconnectivity of components of ETI**.** Although some components of the process were identified to be differentially expressed also by analysis of homogenized tissue in our previous studies (Baebler et al. 2014), the complexity of interactions could not be predicted from analysis of homogenized tissue, indicating the importance of implemented approach.

One characteristic feature of the ETI is rapid and intense production of ROS (Herrera-Vasquez et al., 2015). In immunity, ROS are generated in two phases. The first, low-amplitude and transitory phase occurs within minutes after infection. ROS generated at this stage is mostly apoplastic, tightly linked to posttranslational activation of plasma-membrane RBOH NADPH oxidases (e.g., AtRBOHD and AtRBOHF) and cell-wall peroxidases and is attributed to PTI (Torres, 2010; Shapiguzov et al., 2012; Kadota et al., 2019). The second, high-amplitude and sustained phase takes place a few hours after infection and depends on ROS generation in multiple compartments, including the apoplast, chloroplasts, mitochondria, and peroxisomes. This second phase is linked to ETI and requires transcriptional activation of *RBOH* genes (Shapiguzov et al., 2012).

The role of RBOH proteins as the principal generator of ROS after pathogen attack was, using mutant and transgenic lines, mostly studied in compatible interactions with bacterial and oomycete pathogens (Allan et al., 2001; Torres et al., 2002; Yoshioka et al., 2003; Peer et al., 2011), but also in symbiotic interaction with rhizobia (Yu et al., 2018). Our spatiotemporal analysis of responses revealed that potato *RBOHD* (orthologue of *AtRBOHD*) is transcriptionally induced at the border region between virus-replicating and healthy cells around the cell death zone in ETI (Figure 4). Several studies pointed to the essential role of ROS also in virus resistance in HR (reviewed in Hernández et al. 2015), including one of the most studied viral pathosystems, TMV-tobacco interaction (Mur et al., 1997; Liao et al., 2015). While the induction of *RBOHD* in potato-PVY interaction was shown before (Otulak-Kozieł et al., 2019), its role in ETI was not functionally studied. We confirmed for the first time its essential role in ETI as RBOHD silenced transgenic plants were not able to arrest the virus spread (Figure 6). Besides the effect on cell to cell movement, both SA and *RBOHD* have also an effect on the efficiency of viral

infection. The number of established foci of viral infection was the highest in NahG plants followed by RBOHD silenced plants, whereas lowest number of viral foci appeared in non-transgenic plants (Figure 6). These results could imply higher importance of SA in ETI signaling compared to RBOHD, one however has to note that NahG reduces the amounts of SA to less than 10% of native values (data not shown) while *RBOHD* is, in our transgenic lines, silenced to approximately 50% of its native transcriptional activity (Figure 6).

Although the oxidative burst following pathogen recognition occurs in the apoplast, being generated mostly by RBOH proteins and cell wall peroxidases, pathogen-induced ROS can be also produced in other cellular compartments like mitochondria, chloroplasts and peroxisomes (reviewed in Mignolet-Spruyt et al., 2016; Sharma et al., 2012). Our comparative analysis of NT and NahG genotypes shows that the extensive production of ROS corresponds to the spread of the virus and/or PCD (Figure 5, Lukan et al. 2018). Extensive ROS response in later stages of infection is most likely of non-apoplastic origin, as ROS production corresponded to the expression of *RBOH* genes in NT but not in NahG plants (Figures 6 and 7). This is also supported by the expression pattern of ROS quenchers CAT1 and PRX28, which are induced more distantly from the virus foci in NahG compared to NT plants (Figure 4). As SA was shown to be required for generation of mitochondrial ROS during pathogen infection (Liao et al., 2015), chloroplasts are its most probable source in our system. Transcriptional down-regulation of photosynthesis genes leads to generation of chloroplast ROS, which were proposed as a signal orchestrating PCD (Zurbriggen et al., 2010; Su et al., 2018). In our pathosystem transcriptional down-regulation of photosynthesis genes was observed (Baebler et al. 2014) thus we can assume that, similarly, chloroplastic ROS is generated. Our results of H_2O_2 staining (Figure 5) are in agreement with the hypothesis that chloroplastic ROS stimulates localised cell death.

The studies in Arabidopsis could not unambiguously determine the role of SA in initiation of pathogen-induced PCD. In some pathosystems PCD can be regulated by SA, but not in all (Huysmans et al., 2017; Radojičić et al., 2018). Here we determined that features of HR PCD are not dependent on SA in our studied pathosystem (Figure 3, Figure 6D). Moreover, this study provides the first detailed spatiotemporal ultrastructural analysis of HR-type of PCD in potato following *Potyvirus* infection. We

observed typical features of necrotic and vacuolar PCD on the border of early and fully developed lesions (Figure 3). Similar features were previously observed in different pathosystems resulting either in susceptible or resistant plant-*Potyvirus* interaction (Hinrichs-Berger et al., 1999; Otulak and Grazyna, 2012; Zielińska et al., 2012; Choi et al., 2016), in line with the hypothesis that mechanisms of PCD are independent of resistance mechanism (Künstler et al., 2016). This is also in line with recent study revealing that activation of NLR proteins can directly lead to cell lysis through insertion of resistosome into plasma membrane (Wang et al., 2019).

ROS were proposed to be a central component of a self-amplifying loop that regulates the interaction balance between different phytohormones such as SA, JA and ET (reviewed in Torres, 2010). SA regulates RBOHD-dependent ROS production in Arabidopsis (reviewed in Liu and He, 2016). The same is true for our pathosystem as induction of *RBOHD* expression was in NahG plants significantly reduced after PVY inoculation (Figure 6, Supplemental Figure 10, Supplemental Dataset 1). In Arabidopsis, RBOHD knockout mutant plants accumulated higher levels of SA following interaction with pathogen (Pogany et al., 2009). On the other hand, Chaouch et al. (2012) did not detect any difference in SA accumulation in RBOHD mutant compared to wild type Arabidopsis (Chaouch et al. 2012). We showed that in potato-PVY interaction, SA biosynthesis is not controlled by RBOHD generated ROS as the concentration of SA in transgenic plants with silenced RBOHD did not differ significantly from SA concentration in NT plants at the site of viral foci. RBOHD is however involved in spatial control of its accumulation (Figure 7) confirming the existence of regulatory feedback loops. Indeed, *UDP-glucosyltransferase* (*UGT76D1*) was identified as a component of the feedback activation loop of SA biosynthesis (Huang et al., 2018) and our results show that it is repressed by RBOHD signalling, explaining the spatiotemporal regulation of SA accumulation (Figure 7, Figure 7C).

We also show that several other genes are directly under the regulation of SA. Besides *RBOHD*, spatial responses of *BGLU2*, *HSP70*, *ACX3* and *TRXH* were completely abolished in the SA-deficient line (Figures 3, 5, 6). Interestingly, in several genes, SA deficiency only modulated the response. One of such genes is *PR1B* which is in Arabidopsis generally considered to be activated through SA signaling module (Tsuda et al., 2013). Also, *ERF1*, which encodes a transcription factor involved in ethylene

signaling, and some redox state-related genes (*PRX28*, *RBOHA* and *CAT1*) were spatially responding differently in the absence of SA, their expression peaking further away from the lesion compared to NT plants (Figures 3 and 6).

In an efficient ETI plant needs to block the pathogen multiplication and its spread, and at the same time limit the extent of damaged tissue and energy consumption. Thus tight spatial regulation of this processes is of upmost importance. It has been long assumed that positive regulators act at the HR site and negative regulators in the surrounding areas, but the molecular evidence for this premise is mostly lacking due to lack of functional zonation studies (Huysmans et al., 2017). We here performed a spatiotemporal analysis and showed that RBOHD and SA regulate the ETI response in a diverse manner, probably through multiple regulatory loops leading to fine-tuning of both spatial and temporal response. This delicate balance is ultimately leading to the outcome of interaction favorable for the crop.

METHODS

Plant material

Potato (*Solanum tuberosum* L.) plants cv. Rywal and NahG-Rywal (Baebler et al. 2014) and derived transgenic lines (see below) were grown in stem node tissue culture. Two weeks after node segmentation, they were transferred to soil in a growth chamber and kept under controlled environmental conditions as described elsewhere ((Baebler et al., 2009). After three to four weeks of growth in soil, the potato plants were inoculated with PVY^{NTN} (isolate NIB-NTN, AJ585342), $PVY^{N\text{-}Wilga}$ (PVYN–Wi; EF558545) or with PVY^{N605}, tagged with green fluorescent protein (Rupar et al. 2015) or mock-inoculated as described by Baebler et al., 2009. Plant material for sampling initial virus foci (see below) was prepared using PVY^{N605}, tagged with green fluorescent protein (Jakab et al., 1997; Dietrich and Maiss, 2003) as described by Baebler et al., 2014.

qPCR gene expression analysis in tissue sections

For gene expression analyses lesions at three different stages were sampled (see Figure 1A). For each experimental group, 5-10 lesions from different plants per experiment (Supplemental Table 3,

Supplemental Dataset 1) were sampled. For each lesion, 4 tissue sections were sampled: A) lesion, or in the case of initial viral foci tissue surrounding the site of virus multiplication, and B, C, D) consecutive 1 mm strips distal to the lesion (Figure 1A). In mock-inoculated plants, 4 adjacent tissue sections of the same sizes as in inoculated leaves were excised from different plants. Tissue sections were stored in 100 µl of RNAlater RNA Stabilization Solution (Thermo Fisher Scientific). Altogether 5 independent experiments were performed (see Supplemental Table 3), each comprising of ca. 20 plants per experimental group.

Standard gene expression analysis procedures were optimized for the analysis of small leaf sections. RNA was isolated from fixed tissue sections using the RNeasy Plant Micro Kit (Qiagen) according to the manufacturer's instructions with prior homogenization using Tissue Lyser (Qiagen). DNase-treated (0.5 µl DNase per µg RNA; Qiagen) total RNA was quality controlled using 2100 Bioanalyzer and RNA 6000 Pico LabChip Kit (Agilent Technologies) and then reverse transcribed using the High Capacity cDNA Reverse Transcription Kit (Thermo Fisher Scientific).

Samples were analyzed in the set-up for quantitative PCR (qPCR) as previously described (Petek et al., 2014). Expression of 23 genes involved in different steps of immune signaling was analyzed and normalized to the expression of two validated reference genes *COX* and *18S* (see Supplemental Table 4 for primer and probe information). The standard curve method was used for relative gene expression quantification using quantGenius (http://quantgenius.nib.si; Baebler et al., 2017).

Statistical modelling of tissue section qPCR gene expression data

Prior to statistical analysis of tissue sections gene expression dataset, data from lesions without viral amplification detected in section A (necrosis due to mechanical inoculation) was filtered out. Relative gene expression values were next Standardized to 97th percentile. Multiple linear regression method, as implemented in R Stats package (R Core Team, 2017), was used to fit a quadratic polynomial model, with genotype as factor and position (tissue section) as a factor or numeric distance from the position A (initial viral foci tissue surrounding). Analysis of variance was used to analyze the effects of position and genotype on gene expression. For each analyzed gene, spatial expression profiles were determined

and plotted with 95% confidence intervals. For early visible lesions data, calculations were done for both perpendicular directions and their average, respectively. Expression changes between genotypes in different time post inoculation were further visualized using coefficient plots with linear coefficients displayed on the x-axis and quadratic coefficients on the y-axis. Significance of comparisons between the levels of the factors was obtained through contrast method as implemented in R package limma.

Relative expression measurements of 13 genes (*13-LOX*, *9-LOX*, *ACX3*, *CAT1*, *ERF*1, *LSD1*, *MC3*, *PRX28*, *PR1B*, *RBOHA*, *RBOHC*, *RBOHD*, *TRXH*; see Supplemental Table 4 for full gene names and gene IDs) and PVY, that had qPCR measurement at all time points, were chosen for the integrative analysis. Multiple linear regression method was used in a similar manner with the addition of the new factor - sampling time. Analysis of variance, as implemented in R car package, was used to analyze the effects of all three factors. Contrasts were again calculated using R package limma.

Gene expression in whole leaves

For the gene expression analysis in whole leaves of different genotypes, including newly constructed transgenic lines (see experimental setups below), whole leaves were sampled. RNA was isolated, reverse transcription and qPCR was performed as described previously (Baebler et al. 2014), with normalization to COX only. Where applicable, t-test statistics (Excel) was used to compare treatments.

RNA-Seq analysis in tissue sections

For RNA-seq, early visible lesions were sampled from $PVY^{N\text{-}Wilga}$-inoculated leaves of NT, NahG and shRBOHD (line 14) plants. 30 tissue sections of the lesion (A) and its immediate surrounding (B; Figure 1A) were collected and pooled separately (pool A, pool B). Sections of mock-inoculated plants were prepared as described above and pooled (caa 300 sections per pool). The pools were stored and homogenized as described above. Total RNA was extracted with TRIzol (Invitrogen) and Direct-zol RNA MicroPrep Kit, DNAse treated and purified with RNA Clean & Concentrator kit (both Zymo Research) according to the manufacturer's instructions. Libraries were generated using TruSeq Stranded mRNA Library Prep Kit (Illumina) or SMART-Seq_v4 Ultra Low Input RNA Kit (TaKaRa Bio) and Nextera XT kit (Illumina). RNA-seq was performed on the HiSeq platform (Illumina) using 150-bp paired-end reads at

Novogene or LC Sciences. Reads were trimmed of low-quality bases (phred quality score > 20), ambiguous nucleotides and adapter sequences with the CLC Genomics Workbench 12.0 (Qiagen)). Merging of overlapping pairs, mapping the reads to the potato genome and read counting were performed using CLC Genomics Workbench 12.0 (read alignment parameters: length fraction: 0.9, similarity fraction: 0.9, maximum number of hits for a read: 1) and STAR (read alignment parameters: outFilterMultimapNmax: 10, outFilterMismatchNoverReadLmax: 0.05, limitSjdbInsertNsj: 30000) (http://code.google.com/p/rna-star/; Dobin et al., 2013). Differential expression analysis was performed in R (R Core Team, 2013; version 3.2.2), using the R package limma (Ritchie et al., 2015). In short, gene counts with a baseline expression level of at least 50 counts in at least three samples were TMM-normalized (edgeR package; Robinson et al., 2010) and analyzed using voom function (Law et al., 2014). To identify differentially expressed genes the empirical Bayes approach was used and the resultant p-values were adjusted using Benjamini and Hochberg's (FDR) method. Adjusted p-values below 0.05 were considered statistically significant. Raw and normalized RNA-seq data was deposited to GEO (accession number GSE142002).

Gene set enrichment analysis (GSEA; Subramanian et al., 2005) was performed to search for groups of genes involved in the same processes that were significantly (FDR corrected Q-value < 0.05) altered by virus inoculation, using MapMan ontology as the source of the gene sets.

Construction of short hairpin RNA transgenics

Primers were designed based on consensus sequence obtained by sequence alignment of sequences of *RBOHD* genes (Sotub06g025550 and Sotub06g025580) (Supplemental Figure 14). Total RNA was isolated from leaves of potato plants of cv. Rywal, DNase-treated and reverse transcribed as described in Baebler et al. 2014. Resulting cDNA was used as a template for the amplification of the 436 bp-long fragment of *RBOHD* gene using Phusion® High-Fidelity DNA Polymerase (NEB) using touch down protocol and RBOHD_F/RBOHD_R primers (Supplemental Figure 14). The product was cloned into pENTR D-TOPO plasmid using pENTR™/D-TOPO® Cloning Kit (Thermo Fisher Scientific) and sequenced using M13_F/M13_R primers. The fragment was further transferred to pH7GWIWG2 using *Gateway*™ *LR* Clonase™ II enzyme mix (Thermo Fisher Scientific), sequenced using T35S_F/CmR_F primers

(Supplemental Figure 14) and electroporated into *Agrobacterium tumefaciens* LBA4404 (Eppendorf Electroporator 2510) following manufacturer's protocol at 2000 V. Stem internodes from in vitro plantlets of cv. Rywal were transformed as described elsewhere (Baebler et al. 2014). Well-rooted hygromycin-resistant plants were sub-cultured to produce plantlets of the independently transformed lines. Silencing efficacy was analyzed in one leaf per transgenic line by qPCR using shRBOHD primers (Supplemental Table 4) as a target as described above.

Phenotypisation

To follow lesions appearance in upper non-inoculated leaves of cv. Rywal, NahG-Rywal and two short hairpin transgenic lines with silenced RBOHD (lines 13 and 14), plants were inoculated with PVY^{N}-GFP or mock-inoculated. Lesions were counted on three virus-inoculated leaves from 3 dpi to 14 dpi (see Supplemental Dataset 5 for numbers of tested plants for each experiment). Numbers of lesions was calculated per cm^2 of leaf area.

For the analysis of viral amount, inoculated leaves of the same genotypes as listed above were sampled 6 days post mock or PVY^{N}-GFP inoculation, while non-inoculated leaves were sampled 24 and 39 dpi. Sample preparation and qPCR analysis were performed as described above using PVY as a target gene. For each genotype 1-3 leaves from up to 5 plants were analyzed. The experiment was repeated three times.

To compare lesion diameter between genotypes and viral strains, Rywal and NahG-Rywal plants were inoculated with $PVY^{N\text{-}Wilga}$ and PVY^{NTN}. The diameter of the lesion was measured on images of individual leaves in Adobe Photoshop CS3 and Standardized to leaf diameter. The experiment was repeated twice.

H_2O_2 staining

Rywal and NahG-Rywal plants were inoculated with PVY^{NTN} as described above. The inoculated leaves were sampled 3 to 8 days after inoculation and stained with DAB (3,3'-diaminobenzidine, Sigma-Aldrich) staining solution, prepared by dissolving 1 mg mL^{-1} DAB in 10 mM aqueous HCl (pH 3.8) and

adding 30 mM Na_2HPO_4 and 0.05% Tween-20. The three inoculated leaves from three plants per genotype and treatment were cut at the base and photographed with an EOS 1000D camera (Canon). Leaves were immersed in the DAB staining solution, vacuum infiltrated and incubated at room temperature in darkness for 5 hours. Leaves were cleared in two changes of boiling ethanol for 5 minutes each to remove the chlorophyll and stored in 4:1 mixture of absolute ethanol and glycerol. Leaves were arranged in transparencies and scanned with a flatbed scanner (CanoScan 4400F, Canon). Diameters of lesions and DAB staining areas were measured on spatially calibrated images in Fiji (Schindelin et al., 2012). The difference in diameter of lesion and DAB area was measured in each individual lesion. Data was analyzed in R version 3.5.0 (R Core Team, 2018), statistical significance was tested with ANOVA and Tukey's post-hoc test ($p = 0.05$).

Fluorescence microscopy

When imaging initial viral foci (PVY^{N}-GFP), leaf sections were analyzed using fluorescence stereo microscope Nikon SMZ1500 (Nikon Instruments B.V. Europe) with a range of magnification from 0.75x to 11.25x and 10x eyepieces. GFP was detected using a GFP-B band pass filter set (excitation: 480/40 nm; emission: 535/50 nm).

Transmission electron microscopy

Ultrastructural changes following PVY^{NTN} and $PVY^{N\text{-}Wilga}$ inoculation of the cells in and around the early visible and fully developed lesions were observed in Rywal and NahG-Rywal using transmission electron microscopy (TEM). Tissue section with a lesion and surrounding cells was cut from inoculated leaves (Figure 1A) and fixed with 2.5% glutaraldehyde in 0.08 M phosphate buffer, pH 7.2. All samples were postfixed with 1% (w/v) osmium tetroxide and embedded in Agar 100 resin (Agar Scientific). Ultrathin sections were stained with aqueous uranyl-acetate, followed with lead citrate and examined with TEM Philips CM 100 (Eindhoven, The Netherlands), operating at 80 kV. Images were recorded with ORIUS SC 200 or Bioscan 972 CCD camera (Gatanm Inc.), using Digital Micrographe software (Gatan, Inc.). To estimate the lesion size in each genotype, cross sections of the leaves were analyzed by TEM. Averaged lesion size was determined by counting dead cells in diameter of approximately 15 lesions for each genotype.

Hormonal measurements

SA and JA content were determined in non-transgenic cv. Rywal and two short hairpin transgenic lines with silenced *RBOHD* (lines 13 and 14) 4 dpi after $PVY^{N\text{-}Wilga}$ or mock- inoculation. 60-130 sections containing initial virus foci (section A) and surrounding tissue (section B) were sampled from the third inoculated leaf from 6-8 plants of each genotype. Hormones were isolated and measured by gas chromatography coupled with mass spectrometry (GC-MS) as described by Križnik et al., (2017).

SUPPLEMENTAL DATA

- Supplemental Figure 1: Symptoms appear systemically if Ny-gene-conferred ETI is perturbed in SA signaling. Supports Figure 1.
- Supplemental Figure 2: Lesion diameter is two-fold larger in NahG compared to NT plants following inoculation with PVYN-Wilga or PVYNTN. Supports Figure 1.
- Supplemental Table 1: Gene expression changes of selected genes in whole leaves. Supports Figure 1.
- Supplemental Figure 3: Transcriptional response of immune signaling-related genes and relative viral RNA abundance is similar after inoculation with different viral strains. Supports Figure 2.
- Supplemental Figure 4: Initial foci sampling. Supports Figure 1.
- Supplemental Figure 5: Spatial profile of transcriptional response of selected genes in the early stages of viral infection. Supports Figure 2.
- Supplemental Figure 6: Consistent spatial gene expression of immune signaling genes around early visible lesions. Supports Supplemental Figure 9 and Figure 4.
- Supplemental Figure 7: Spatial response of the genes related to cell death process can be detected already at the time of early visible lesions. Supports Figures 2 and 3.
- Supplemental Figure 8: Programmed cell death in the centre of fully developed lesion after PVY infection. Supports Figure 3.
- Supplemental Figure 9: 9-LOX and 13-LOX branches of the oxylipin pathway respond differentialy in potato ETI against PVY.
- Supplemental Figure 10: Virus is present in symptomatic non-inoculated leaves of plants of RBOHD-silenced transgenic lines. Supports Figure 6.
- Supplemental Figure 11: Lesions on inoculated leaves of plants of different genotypes. Supports Figure 6.
- Supplemental Table 2: Sample information and salicylic acid content in tissue sections of NT and two shRBOHD lines. Supports Figure 7.

- Supplemental Figure 12: Spatial transcriptional response is similar in shRBOHD and NahG genotypes. Supports Table 1.
- Supplemental Figure 13: Spatial expression of UDP-glucosyltransferase (UGT76D1) in different genotypes. Supports Figure 7.
- Supplemental Table 3: Sampling for spatiotemporal gene expression analyses. Supports Methods.
- Supplemental Table 4: Selected genes and corresponding primers and probes sequences for expression analyses with quantitative PCR. Supports Methods.
- Supplemental Figure 14. Construction of short hairpin RNA transgenics. Supports Methods.
- Supplemental Dataset 1: Sample information and gene expression of selected genes in lesion sections.
- Supplemental Dataset 2. Statistical modeling of tissue section gene expression data.
- Supplemental Dataset 3: Spatiotemporal gene expression of immune signaling genes.
- Supplemental Dataset 4: 3D animated spatial gene expression of immune signaling genes around early visible lesions.
- Supplemental Dataset 5: Number of lesions on inoculated leaves of different potato genotypes following PVY inoculation.
- Supplemental Dataset 6: Gene expression changes of Rywal, NahG and shRBOHD genotypes following PVYN-Wilga infection determined by RNA-Seq.

ACKNOWLEDGEMENTS

The research was financially supported by the Slovenian Research Agency (research core funding No. P4-0165 and projects J4-7636, J4-1777 and 1000-15-0105) and Grant no. 2017/27/B/N29/01803 from NSC, Poland. The authors thank Dr. John Carr for critical review of the manuscript and Maja Gnezda, Neža Turnšek and Lidija Matičič for technical assistance.

AUTHOR CONTRIBUTIONS

ŠB, MPN, KG, TL, JH designed the research; ŠB, MPN, KG, TL, MTŽ, AK, KS, BD, AC, SP, KM, MK performed research; TL, ŠB, AK, AB, MZ, KG, MK analyzed data; TL, ŠB, KG wrote the paper.

REFERENCES

Allan, a C., Lapidot, M., Culver, J. N., and Fluhr, R. (2001). An early tobacco mosaic virus-induced oxidative burst in tobacco indicates extracellular perception of the virus coat protein. *Plant Physiol.* **126**:97–108.

Antoniw, J. F., and White, R. F. (1986). Changes with time in the distribution of virus and PR protein around single local lesions of TMV infected tobacco. *Plant Mol. Biol.* **6**:145–149.

Aranda, M. A., Escaler, M., Wang, D., and Maule, A. J. (1996). Induction of HSP70 and polyubiquitin expression associated with plant virus replication. *Proc. Natl. Acad. Sci. USA* **93**:15289–15293.

Baebler, Š., Krečič-Stres, H., Rotter, A., Kogovšek, P., Cankar, K., Kok, E. J., Gruden, K., Kovač, M., Žel, J., Maruša, P.-N., et al. (2009). PVYNTN elicits a diverse gene expression response in different potato genotypes in the first 12 h after inoculation. *Mol. Plant Pathol.* **10**:263–275.

Baebler, Š., Witek, K., Petek, M., Stare, K., Tušek-Žnidarič, M., Pompe-Novak, M., Renaut, J., Szajko, K., Strzelczyk-Zyta, D., Marczewski, W., et al. (2014). Salicylic acid is an indispensable component of the Ny-1 resistance-gene-mediated response against Potato virus y infection in potato. *J. Exp. Bot.* **65**:1095–1109.

Baebler, Š., Svalina, M., Petek, M., Stare, K., Rotter, A., Pompe-Novak, M., and Gruden, K. (2017). QuantGenius: Implementation of a decision support system for qPCR-based gene quantification. *BMC Bioinformatics* **18**:276.

Baggs, E., Dagdas, G., and Krasileva, K. V (2017). ScienceDirect NLR diversity, helpers and integrated domains: making sense of the NLR IDentity. *Curr. Opin. Plant Biol.* **38**:59–67.

Balint-Kurti Peter (2019). The plant hypersensitive response: concepts, control and consequences. *Mol. Plant Pathol.* **20**:1163–1178.

Betsuyaku, S., Katou, S., Takebayashi, Y., Sakakibara, H., Nomura, N., and Fukuda, H. (2018). Salicylic Acid and Jasmonic Acid Pathways are Activated in Spatially Different Domains Around the Infection Site During Effector-Triggered Immunity in Arabidopsis thaliana. *Plant Cell Physiol* **59**:8–16.

Breen, S., Williams, S. J., Outram, M., Kobe, B., and Solomon, P. S. (2017). Emerging Insights into the Functions of Pathogenesis- Related Protein 1. *Trends Plant Sci.* **22**:871–879.

Calil, I. P., and Fontes, E. P. B. (2017). Plant immunity against viruses: Antiviral immune receptors in focus. *Ann. Bot.* **119**:711–723.

Chaouch, S., Queval, G., and Noctor, G. (2012). AtRbohF is a crucial modulator of defence-associated metabolism and a key actor in the interplay between intra-cellular oxidative stress and pathogenesis responses in Arabidopsis. *Plant J.* **69**:613–627.

Chivasa, S., and Carr, J. P. (1998). Cyanide Restores N Gene-Mediated Resistance to Tobacco Mosaic Virus in Transgenic Tobacco Expressing Salicylic Acid Hydroxylase. *Plant Cell* **10**:1489–1498.

Chivasa, S., Murphy, a. M. A., Naylor, M., and Carr, J. P. (1997). Salicylic Acid Interferes with Tobacco Mosaic Virus Replication via a Novel Salicylhydroxamic Acid-Sensitive Mechanism. *Plant Cell* **9**:547–557.

Choi, D., Park, J., Oh, S., and Cheong, H. (2016). Autophagy induction in tobacco leaves infected by potato virus YO and its putative roles. *Biochem. Biophys. Res. Commun.* **474**:606–611.

Dickman, M. B., and Figueiredo, P. De (2013). Death Be Not Proud — Cell Death Control in Plant Fungal Interactions. *PLoS Pathog.* **9**:e1003542.

Dietrich, C., and Maiss, E. (2003). Fluorescent labelling reveals spatial separation of potyvirus populations in mixed infected Nicotiana benthamiana plants. *J. Gen. Virol.* **84**:2871–2876.

Dobin, A., Davis, C. A., Schlesinger, F., Drenkow, J., Zaleski, C., Jha, S., Batut, P., Chaisson, M., and Gingeras, T. R. (2013). STAR: Ultrafast universal RNA-seq aligner. *Bioinformatics* **29**:15–21.

Dorey, S., Baillieul, F., Pierrel, M., Saindrenan, P., Fritig, B., Biologie, I. De, and Pasteur, U. L. (1997). Spatial and Temporal Induction of Cell Death, Defense Genes, and Accumulation of Salicylic Acid in Tobacco Leaves Reacting Hypersensitively to a Fungal Glycoprotein Elicitor. *MPMI* **10**:646–655.

Escaler, M., Aranda, M. A., Thomas, C. L., and Maule, A. J. (2000). Pea Embryonic Tissues Show Common Responses to the Replication of a Wide Range of Viruses. *Virology* **267**:318–325.

Gantner, J., Ordon, J., Kretschmer, C., Guerois, R., and Stuttmann, J. (2019). An EDS1-SAG101 Complex is Essential for TNL-mediated Immunity in Nicotiana benthamiana. *Plant Cell* **In press**.

Giacomello, S., Salmén, F., Terebieniec, B. K., Vickovic, S., Navarro, J. F., Alexeyenko, A., Reimegård, J., Mckee, L. S., Mannapperuma, C., Bulone, V., et al. (2017). Spatially resolved transcriptome profiling in model plant species. *Nat. Plants* **3**:17061.

Havelda, Z., and Maule, A. J. (2000). Complex Spatial Responses to Cucumber Mosaic Virus Infection in Susceptible Cucurbita pepo Cotyledons **12**:1975–1985.

Herrera-Vasquez, A., Salinas, P., and Holuigue, L. (2015). Salicylic acid and reactive oxygen species interplay in the transcriptional control of defense genes expression **6**:1–9.

Hinrichs-Berger, J., Harfold, M., Berger, S., and Buchenauer, H. (1999). Cytological responses of susceptible and extremely resistant potato plants to inoculation with potato virus Y. *Physiol. Mol. Plant Pathol.* **55**:143–150.

Huang, X. X., Zhu, G. Q., Liu, Q., Chen, L., Li, Y. J., and Hou, B. K. (2018). Modulation of plant salicylic acid-associated immune responses via glycosylation of dihydroxybenzoic acids. *Plant Physiol.* **176**:3103–3119.

Huysmans, M., A, S. L., Coll, N. S., and Nowack, M. K. (2017). Dying two deaths — programmed cell death regulation in development and disease. *Curr. Opin. Plant Biol.* **35**:37–44.

Jakab, G., Droz, E., Brigneti, G., Baulcombe, D., and Malnoe, P. (1997). Infectious in vivo and in vitro transcripts from a full-length cDNA clone of PVY-N605, a Swiss necrotic isolate of potato virus Y. *J. Gen. Virol.* **78**:3141–3145.

Jones, J. D. G., and Dangl, J. L. (2006). The plant immune system. *Nature* **444**:323–329.

Kadota, Y., and Shirasu, K. (2012). The HSP90 complex of plants. *Biochim. Biophys. Acta* **1823**:689–697.

Kadota, Y., Liebrand, T. W. H., Goto, Y., Sklenar, J., Derbyshire, P., Menke, F. L. H., Torres, M., Molina, A., Zipfel, C., Coaker, G., et al. (2019). Quantitative phosphoproteomic analysis reveals common regulatory mechanisms between effector- and PAMP-triggered immunity in plants. *New Phytol.* **221**:2160–2175.

Karasev, A. V., and Gray, S. M. (2013). Continuous and Emerging Challenges of *Potato virus Y* in Potato. *Annu. Rev. Phytopathol.* **51**:571–586.

Križnik, M., Petek, M., Dobnik, D., Ramšak, Ž., and Baebler, Š. (2017). Salicylic Acid Perturbs sRNA-Gibberellin Regulatory Network in Immune Response of Potato to Potato virus Y Infection. *Front. Plant Sci.* **8**:2192.

Künstler, A., Bacsó, R., Gullner, G., Hafez, Y. M., and Király, L. (2016). Staying alive - is cell death dispensable for plant disease resistance during the hypersensitive response? *Physiol. Mol. Plant Pathol.* **93**:75–84.

Law, C. W., Chen, Y., Shi, W., and Smyth, G. K. (2014). Voom: Precision weights unlock linear model analysis tools for RNA-seq read counts. *Genome Biol.* **15**:R29.

Lee, T., Kim, H., and Lee, I. (2015). Network-assisted crop systems genetics: network inference and integrative analysis. *Curr. Opin. Plant Biol.* **24**:61–70.

Liao, Y., Tian, M., Zhang, H., Li, X., Wang, Y., Xia, X., Zhou, J., Zhou, Y., Yu, J., Shi, K., et al. (2015). Salicylic acid binding of mitochondrial alpha-ketoglutarate dehydrogenase E2 affects mitochondrial oxidative phosphorylation and electron transport chain components and plays a role in basal defense against tobacco mosaic virus in tomato. *New Phytol.* **205**:1296–1307.

Liu, Y., and He, C. (2016). Regulation of plant reactive oxygen species (ROS) in stress responses: learning from AtRBOHD. *Plant Cell Rep.* **35**:995–1007.

Lukan, T., Baebler, Š., Maruša, P.-N., Guček, K., Zagorščak, M., Coll, A., and Gruden, K. (2018). Cell Death Is Not Sufficient for the Restriction of Potato Virus Y Spread in Hypersensitive Response-Conferred Resistance in Potato. *Front. Plant Sci.* **9**:168.

Macho, A. P., and Lozano-Duran, R. (2019). Molecular dialogues between viruses and receptor-like kinases in plants. *Mol. Plant Pathol.* **20**:1191–1195.

Maule, A., Leh, V., and Lederer, C. (2002). The dialogue between viruses and hosts in compatible interactions. *Curr. Opin. Plant Biol.* **5**:279–284.

Mignolet-Spruyt, L., Xu, E., Idänheimo, N., Hoeberichts, F. A., Mühlenbock, P., Brosché, M., Van Breusegem, F., and Kangasjärvi, J. (2016). Spreading the news: subcellular and organellar reactive oxygen species production and signalling. *J. Exp. Bot.* **67**:3831–3844.

Mur, L. A. J., Bi, Y.-M., Darby, R. M., Firek, S., and Draper, J. (1997). Compromising early salicylic acid accumulation delays the hypersensitive response and increases viral dispersal during lesion establishment in TMV-infected tobacco. *Plant J.* **12**:1113–1126.

Mur, L. A. J., Kenton, P., Lloyd, A. J., Ougham, H., and Prats, E. (2008). The hypersensitive response; The centenary is upon us but how much do we know? *J. Exp. Bot.* **59**:501–520.

Otulak-Kozieł, K., Kozieł, E., and Valverde, R. A. (2019). The respiratory burst oxidase homolog D (RbohD) cell and tissue distribution in potato-potato virus Y (PVYNTN) hypersensitive and susceptible reactions. *Int. J. Mol. Sci.* **20**:2741.

Otulak, K., and Grazyna, G. (2012). Cytopathological Potato virus Y structures during Solanaceous plants infection. *Micron* **43**:839–850.

Peer, M., Bach, M., Mueller, M. J., and Waller, F. (2011). Free sphingobases induce RBOHD-dependent reactive oxygen species production in Arabidopsis leaves. *FEBS Lett.* **585**:3006–3010.

Petek, M., Rotter, A., Kogovšek, P., Baebler, Š., Mithöfer, A., and Gruden, K. (2014). Potato virus Y infection hinders potato defence response and renders plants more vulnerable to Colorado potato beetle attack. *Mol. Ecol.* **23**:5378–5391.

Piquerez, S. J. M., Harvey, S. E., Beynon, J. L., and Ntoukakis, V. (2014). Improving crop disease resistance: lessons from research on Arabidopsis and tomato. *Front. Plant Sci.* **5**:1–13.

Pogany, M., von Rad, U., Grun, S., Dongo, A., Pintye, A., Simoneau, P., Bahnweg, G., Kiss, L., Barna, B., and Durner, J. (2009). Dual Roles of Reactive Oxygen Species and NADPH Oxidase RBOHD in an Arabidopsis-Alternaria Pathosystem. *Plant Physiol.* **151**:1459–1475.

Radojičić, A., Li, X., and Zhang, Y. (2018). Salicylic Acid: A Double-Edged Sword for Programed Cell Death in Plants. *Front. Microbiol.* **9**:1133.

Ramšak, Ž., Coll, A., Stare, T., Tzfadia, O., Baebler, Š., Peer, Y. Van De, and Gruden, K. (2018). Network Modeling Unravels Mechanisms of Crosstalk between Ethylene and Salicylate Signaling in Potato. *Plant Physiol.* **178**:488–499.

Ritchie, M. E., Phipson, B., Wu, D., Hu, Y., Law, C. W., Shi, W., and Smyth, G. K. (2015). Limma powers differential expression analyses for RNA-sequencing and microarray studies. *Nucleic Acids Res.* **43**:e47.

Robinson, M. D., McCarthy, D. J., and Smyth, G. K. (2010). edgeR: A Bioconductor package for differential expression analysis of digital gene expression data. *Bioinformatics* **26**:139–140.

Rupar, M., Faurez, F., Tribodet, M., Gutierrez-Aguirre, I., Delaunay, A., Glais, L., Kriznik, M., Dobnik, D., Gruden, K., Jacquot, E., et al. (2015). Fluorescently tagged Potato virus Y: a versatile tool for functional analysis of plant-virus interactions. *Mol. plant-microbe Interact. MPMI* **28**:739–750.

Schindelin, J., Arganda-carreras, I., Frise, E., Kaynig, V., Pietzsch, T., Preibisch, S., Rueden, C., Saalfeld, S., Schmid, B., Tinevez, J., et al. (2012). Fiji - an Open Source platform for biological image analysis. *Nat Methods* **9**:1–15.

Scholthof, K. B. G., Adkins, S., Czosnek, H., Palukaitis, P., Jacquot, E., Hohn, T., Hohn, B., Saunders, K., Candresse, T., Ahlquist, P., et al. (2011). Top 10 plant viruses in molecular plant pathology. *Mol. Plant Pathol.* **12**:938–954.

Shapiguzov, A., Julia, P., Wrzaczek, M., and Kangasjärvi, J. (2012). ROS-talk – how the apoplast, the chloroplast, and the nucleus get the message through. *Front. Plant Sci.* **3**:292.

Sharma, P., Jha, A. B., Dubey, R. S., and Pessarakli, M. (2012). Reactive Oxygen Species, Oxidative Damage, and Antioxidative Defense Mechanism in Plants under Stressful Conditions. *Jounal Bot.* **2012**:217037.

Shulse, C. N., Cole, B. J., Ciobanu, D., Malley, R. C. O., Brady, S. M., Dickel, D. E., Shulse, C. N., Cole, B. J., Ciobanu, D., Lin, J., et al. (2019). High-Throughput Single-Cell Transcriptome Profiling of Plant Cell Types. *Cell Rep.* **27**:2241–2247.

Su, J., Yang, L., Zhu, Q., Wu, H., He, Y., Liu, Y., Xu, J., Jiang, D., and Zhang, S. (2018). Active photosynthetic inhibition mediated by MPK3/MPK6 is critical to effector-triggered immunity. *PLoS Biol.* **16**:e2004122.

Subramanian, A., Tamayo, P., Mootha, V. K., Mukherjee, S., Ebert, B. L., Gillette, M. A., Paulovich, A., Pomeroy, S. L., Golub, T. R., Lander, E. S., et al. (2005). Gene set enrichment analysis: A knowledge-based approach for interpreting genome-wide expression profiles. *Proc. Natl. Acad. Sci. U. S. A.* **102**:15545–15550.

Szajko, K., Chrzanowska, M., Witek, K., Strzelczyk-Zyta, D., Zagórska, H., Gebhardt, C., Hennig, J., and Marczewski, W. (2008). The novel gene Ny-1 on potato chromosome IX confers hypersensitive resistance to Potato virus Y and is an alternative to Ry genes in potato breeding for PVY resistance. *Theor. Appl. Genet.* **116**:297–303.

Torres, M. A. (2010). ROS in biotic interactions. *Physiol. Plant.* **138**:414–429.

Torres, M. A., Dangl, J. L., and Jones, J. D. G. (2002). Arabidopsis gp91phox homologues AtrbohD and AtrbohF are required for accumulation of reactive oxygen intermediates in the plant defense response. *Proc. Natl. Acad. Sci.* **99**:517–522.

Verma, V., Ravindran, P., and Kumar, P. P. (2016). Plant hormone-mediated regulation of stress responses. *BMC*

Plant Biol. **16**:86.

Wang, J., Hu, M., Wang, J., Qi, J., Han, Z., Wang, G., Qi, Y., Wang, H. W., Zhou, J. M., and Chai, J. (2019). Reconstitution and structure of a plant NLR resistosome conferring immunity. *Science (80-.).* **364**:eaav5870.

Yang, C., Guo, R., Jie, F., Nettleton, D., Peng, J., Carr, T., Yeakley, J. M., Fan, J., and Whitham, S. A. (2007). Spatial Analysis of Arabidopsis thaliana Gene Expression in Response to Turnip mosaic virus Infection. *MPMI* **20**:358–370.

Yoshioka, H., Numata, N., Nakajima, K., Katou, S., Kawakita, K., Rowland, O., Jones, J. D. G., and Doke, N. (2003). Nicotiana benthamiana gp91 phox Homologs NbrbohA and NbrbohB Participate in H2O2 Accumulation and Resistance to Phytophthora infestans. *Plant Cell* **15**:706–718.

Yu, H., Xiao, A., Dong, R., Fan, Y., Zhang, X., Liu, C., Wang, C., Zhu, H., Duanmu, D., Cao, Y., et al. (2018). Suppression of innate immunity mediated by the CDPK-Rboh complex is required for rhizobial colonization in Medicago truncatula nodules. *New Phytol.* **220**:425–434.

Zielińska, L., Trzmiel, K., and Jeżewska, A. (2012). Ultrastructural changes in maize leaf cells infected with maize dwarf mosaic virus and sugarcane mosaic virus. *ACTA Biol. CRACOVIENSIA Ser. Bot.* **54**:97–104.

Zurbriggen, M. D., Carrillo, N., and Hajirezaei, M.-R. (2010). ROS signalling in the hypersensitive response. *Plant Signal. Behav.* **5**:393–396.